SCIENCE CHINA Materials ARTICLES

mater.scichina.com link.springer.com

Published online 28 June 2018 | https://doi.org/10.1007/s40843-018-9311-9
Sci China Mater 2019, 62(2): 225–235

High-performance flexible and broadband photodetectors based on PbS quantum dots/ZnO nanoparticles heterostructure

Mingfa Peng, Yongjie Wang, Qingqing Shen, Xinkai Xie, Hechuang Zheng, Wanli Ma, Zhen Wen* and Xuhui Sun*

ABSTRACT **Flexible and broadband photodetectors have drawn extensive attention due to their potential application in foldable displays, optical communications, environmental monitoring, etc. In this work, a flexible photodetector based on the crystalline PbS quantum dots (QDs)/ZnO nanoparticles (NPs) heterostructure was proposed. The photodetector exhibits a broadband response from ultraviolet-visible (UV-Vis) to near infrared detector (NIR) range with a remarkable current on/off ratio of 7.08×10^3 under 375 nm light illumination. Compared with pure ZnO NPs, the heterostructure photodetector shows the three orders of magnitude higher responsivity in Vis and NIR range, and maintains its performance in the UV range simultaneously. The photodetector demonstrates a high responsivity and detectivity of 4.54 A W^{-1} and 3.98×10^{12} Jones. In addition, the flexible photodetectors exhibit excellent durability and stability even after hundreds of times bending. This work paves a promising way for constructing next-generation high-performance flexible and broadband optoelectronic devices.**

Keywords: flexible, broadband, photodetector, PbS quantum dots, ZnO nanoparticles

INTRODUCTION

Photodetectors which can convert incident light into electrical signal have drawn much attention due to their extensive applications, such as optical communications, biological imaging, environmental monitoring, and chemical sensing [1–4]. According to the different wavelength range of detection, the photodetectors can be mainly divided into special wavelength detector and broadband detector [5,6]. The special wavelength photodetectors are desired to distinguish a certain narrow-band light or single wavelength light, which are mainly used in the field of a specific wavelength light detecting and optoelectronic integrated circuits. The broadband photodetectors have been widely used in the field of broadband light communication, wide spectral switches or memory storage because of their spectral detection range from ultraviolet (UV) to infrared (IR). Compared to rigid substrate photodetectors, flexible photodetectors with excellent transparency and flexibility are usually fabricated on bendable plastic substrates [7–9]. In recent years, high-performance flexible photodetectors have drawn much attention in many fields, such as large-area foldable displays, wearable ultraviolet radiation monitoring, and implantable biomedical devices, etc. [10–12]. Many kinds of flexible broadband photodetectors based on pure semiconductors or composite nanostructures have been carefully investigated [13,14]. Recently, some efforts have been made to enhance the performance of the flexible photodetector by forming inorganic AuO_x/graphene and organic/inorganic perovskite/ZnO nanowire hybrid structure [15,16]. However, the active materials (graphene and ZnO nanowires) of the photodevices were synthesized *via* high temperature physical evaporation route. The high energy consumption and complicated fabrication processes of the active materials strongly limit their practical applications. Therefore, it is urgent to fabricate proper nanomaterials with broadband response and easily large-scale assembly in the field of flexible and broadband photodetector.

Institute of Functional Nano and Soft Materials (FUNSOM), Jiangsu Key Laboratory for Carbon-Based Functional Materials and Devices, and Joint International Research Laboratory of Carbon-Based Functional Materials and Devices, Soochow University, Suzhou 215123, China
*Corresponding authors (emails: wenzhen2011@suda.edu.cn (Wen Z); xhsun@suda.edu.cn (Sun X))

Recently, solution-processed colloidal inorganic quantum dot (QD) or nanoparticle (NP) materials for photodetectors exhibited many advantages, including low-temperature solution routing, potentially large-scale manufacturing, and compatibility with inexpensive or bendable substrates [17–20]. Moreover, QDs are in favor of the tunable absorption spectrum by controlling the size of the QDs during the synthesis process [19]. Specifically, lead sulfide (PbS) QDs have been widely employed in photodetectors because of their inherent narrow bandgap (~1.3 eV) and tunable absorption spectra from the near-infrared (NIR) to visible (Vis) [21,22]. So far, PbS QDs as essential photoactive layers have been utilized to construct different kinds of optoelectronic devices, such as p–n junction photodiodes, PIN photodetectors, and solar cells [23–25]. Compared with other semiconductors, ZnO with a room-temperature bandgap of 3.3 eV have attracted extensive attention owing to their easy fabrication process and photosensitivity for UV light detection. [23,26]. Some studies have been done to fabricate different ZnO nanostructures for UV photodetectors and improve their performances [27,28]. However, the performances of single-layer devices are often affected by large dark currents, low on-off ratios, slow light responses and narrow spectral response range [29–31]. To overcome the drawbacks of the single-component nanomaterial devices, hybrid architecture or heterostructure (such as PbS QDs/organic hybrid structure and PbS QDs/1D or 2D inorganic nanostructure) have been developed to improve the performance of the photonic devices [32–34]. Although the PbS QDs/ZnO nanowires hybrid structures were demonstrated in solar cells and photonic devices in recent years [20,22,33], so far, flexible and broadband PbS QDs/ZnO NPs heterostructure based photodetector is still rarely reported.

In this work, the crystalline PbS QDs/ZnO NPs heterostructure based two-terminal contact flexible photodetector was fabricated by photolithography and lift-off technique. Each component of the heterostructure has been well characterized. The optoelectronic properties of the flexible photodetector with broadband light illumination from UV-Vis to NIR (375, 532, 635, 808 and 1,064 nm) were investigated in detail. It exhibits a remarkable current on/off ratio of 7.08×10^3 with 375 nm light illumination as well as a high spectra responsivity and detectivity of 4.54 A W^{-1} and 3.98×10^{12} Jones, respectively. Moreover, the flexible photodetector displays excellent mechanical and electrical stability even after 500 bending cycles. The photoresponse enhancement mechanism of PbS QDs/ZnO NPs heterostructure has also been discussed.

EXPERIMENTAL SECTION

Synthesis and characterization

Synthesis of PbS QDs

The oleate-capped PbS QDs were synthesized *via* a rapid hot injection method by following a reported procedure [35]. Briefly, 10 mmol of lead acetate and 7 g of oleic acid (OA) were dissolved in 60 g of 1-octadecene (ODE) in a three-neck flask by heating the mixture to 100°C under vacuum for 2 h. Then, the solution temperature rose to 120°C and maintained for 1 h under nitrogen. After that, 9 mL of ODE and 1 mL of hexamethyldisilathiane (HMS) were rapidly injected into three-neck flask. The QDs were purified by isopropanol and re-dispersed in hexane and acetone two times. The as-synthesized QDs were stored in a nitrogen filled glove box. Finally, PbS QDs were re-dispersed in hexane (20 mg mL^{-1}) for the device fabrication.

Synthesis of ZnO NPs

ZnO nanoparticles were synthesized according to the literature with some modification [36]. Firstly, 1.48 g zinc acetate dehydrate was added into 62 mL of methanol, and then 0.74 g potassium hydroxide was dissolved in 32 mL of methanol. The pre-prepared potassium hydroxide solution was added to the zinc acetate solution slowly, and kept stirring for 3 h at 60°C. The as-synthesized solution was washed twice with methanol and then centrifuged. Finally, the obtained precipitates were dissolved in 10 mL of chloroform and 10 mL of methanol, and the mixed solution was filtered by a 0.45 μm syringe filter.

Characterization

The morphology and structure of the as-synthesized products were characterized by transmission electron microscopy (TEM, FEI Tecnai G2 F20 S-TIWN) equipped with energy dispersive X-ray spectroscopy (EDS), and X-ray diffraction (XRD, Empryean) with Cu Kα radiation (λ=1.5406 Å). The chemical composition of the as-synthesized products was analysed by X-ray photoelectron spectroscopy (XPS) measurement (Kratos AXIS UltraDLD) using a monochromic Al Kα source (1,486 eV). UV-Vis absorption spectra were recorded by a Perkin Elmer Lambda 750 UV-Vis-near-infrared spectrophotometer. Photoluminescence (PL) measurements were performed on samples pre-prepared on quartz substrates, with a 400 nm Ti:sapphire laser (Coherent, Mira 900,

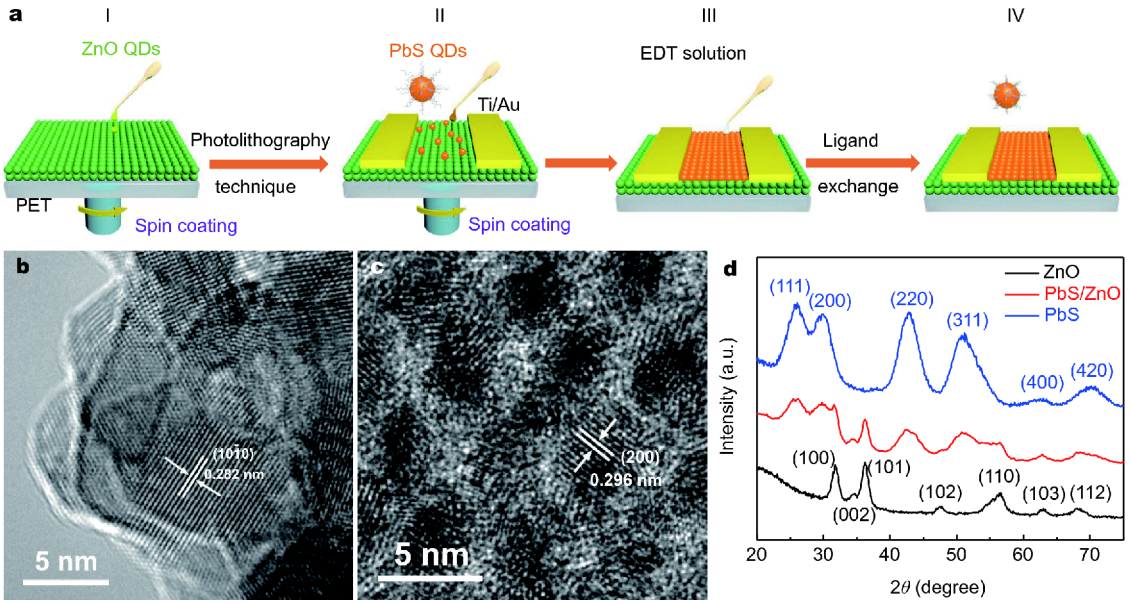

Figure 1 Fabrication the process and characterization of PbS quantum dots (QDs)/ZnO nanoparticles (NPs) heterostructure based photodetector. (a) Schematic illustration of fabrication process of the flexible device. HRTEM image of the as-synthesized (b) ZnO NPs and (c) PbS QDs. (d) XRD spectra of PbS, ZnO and PbS/ZnO heterostructure.

repetition rate 76 MHz) as excitation source. The emission spectra were recorded by a cooled array detector (Andor, iDus 1.7 μm).

Device fabrication and measurements

ZnO NPs film (~100 nm) were deposited on pre-cleaned polyethylene terephthalate (PET) substrates by spin coating at the speed of 2,500 rpm. Ti/Au (10 nm/100 nm) electrodes with a channel length of 5 μm were deposited on top of the ZnO NPs films by photolithography (SUSS Inc., MJB4) and electron-beam evaporation (Kurt. J. Lesker Inc.) method. Then, 20 μL PbS QDs octane (20 mg mL^{-1}) solution was spin-coated on the top of ZnO NPs device at 2,500 rpm for 30 s. For the ligand exchange, the poly(3,4-ethylenedioxythiophene) (EDT)/acetonitrile solution was dropped on the device and maintained for 60 s, followed by rinsing and spinning steps with acetonitrile. These procedures were repeated twice to get a thickness of ~40 nm PbS-EDT layer and all devices were annealed in vacuum at 90°C for 5 min. The *I*–*V* and *I*–*t* characteristic of the photodetectors were recorded by a Keithley SCS-4200 semiconductor characterization system equipped with CASCADE M150 Probe Station. The different wavelength laser light (375 to 1,064 nm) (Changchun Laser Optoelectronics Technology, MW-GX-375, MW-GX-405, MW-GX-532, MW-GX-635, MW-GX-808, and MW-GX-1064) was monochromatic light with light intensity adjustable. The optical power meter (CEL-NP2000) was employed to measure the incident light intensity. The bending repeatability test was performed by an automatic linear motor (Winnemotor, WMUC512075-06-X).

RESULTS AND DISCUSSION

The fabrication process and characterization of the PbS QDs/ZnO NPs heterostructure are shown in Fig. 1. The fabrication process flow of a typical flexible PbS QDs/ZnO NPs heterostructure based photodetector is schematically illuminated in Fig. 1a. Firstly, ZnO NPs were deposited on pre-cleaned PET substrates by spin coating method (Step I). Ti/Au (10 nm/100 nm) electrodes with a distance of 5 μm were deposited on top of the ZnO NPs films by photolithography, electron-beam evaporation and lift-off processes (Step II). Then, the as-synthesized OA capped PbS QDs films were spin-coated on the top of ZnO NPs films. (Step III). After that, the ligand exchange was carried out by dropping the EDT/acetonitrile solution on the complex film (Step IV) and the flexible PbS-EDT/ZnO heterostructure based photodetector can be obtained. The TEM and equipped EDS were primarily employed to characterize the morphology and chemical composition of the as-synthesized products, as shown in Fig. S1. It is obvious that the size distribution of ZnO NPs and PbS QDs are uniform, and the OA capped PbS QDs

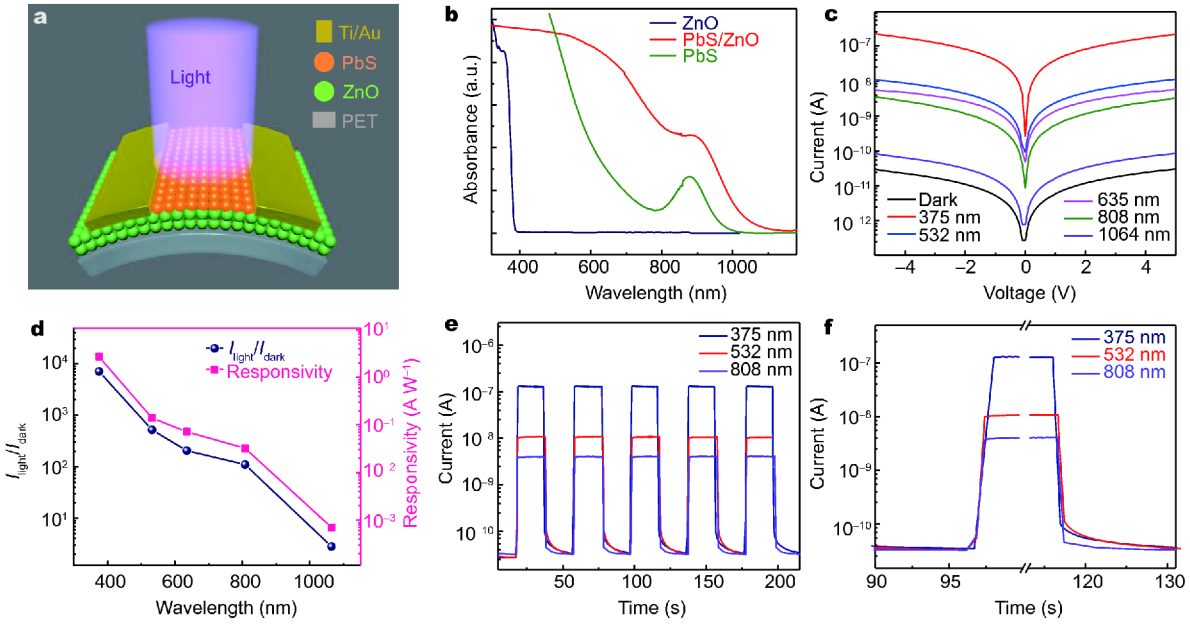

Figure 2 Characterization and performance of the PbS QDs/ZnO NPs heterostructure based photodetector. (a) Schematic view of the two-terminal contact flexible photodetector. (b) UV-Vis spectra of ZnO NPs, PbS QDs/ZnO NPs and PbS QDs. (c) *I*–*V* curve of the PbS/ZnO heterostructure based photodetector under different-wavelength lights or dark conditions. (d) The I_{light}/I_{dark} ratio and responsivity of PbS/ZnO heterostructure based photodetector at different wavelengths from 375 to 1,064 nm at a bias of 5 V. (e) The time-resolved photoresponse of the flexible photodetector under 375, 532 and 808 nm light illumination. (f) The rise time and decay time of the photodetector under 375, 532 and 808 nm light illumination, respectively.

are well-separated (Fig. S1a, c). The EDS analysis reveals that the NPs (QDs) are composed of zinc and oxygen (lead and sulfur) with an atomic ratio close to 1:1 (1:1) (Fig. S1b, d). The XPS results further confirmed the chemical composition of the PbS QDs and ZnO NPs (Figs. S2, S3). The HRTEM images exhibit that the average diameters of the ZnO NPs and PbS QDs are ~5 nm and ~3 nm, respectively (Fig. 1b, c). The lattice fringe spacings are observed to be 0.282 and 0.296 nm, corresponding to the (10−10) plane for ZnO and (200) plane for PbS, respectively. The XRD patterns of the as-prepared ZnO and PbS films reveal that the products can be attributed to hexagonal structure ZnO (a=3.25 Å, c =5.21 Å, JCPDS card 01-070-2551) and cubic structure PbS (a=5.93 Å, c=5.93 Å, JCPDS card 01-078-1901) with uniformly compositions (Fig. 1d). The XRD results further confirm the heterostructures are composed of crystalline ZnO and PbS.

The characterization and performance of the flexible PbS QDs/ZnO NPs heterostructure based photodetector are shown in Fig. 2. The schematic illustration displays a two-terminal contact flexible photodetector, with PbS QDs/ZnO NPs as building blocks, PET as substrate and Ti/Au as metal electrodes (Fig. 2a). Fig. S4 displays the SEM image of the flexible photodetector. The cross-sectional SEM image (Fig. S5) shows that the clear interface of PbS/ZnO heterostructure is tightly integrated. The UV-Vis absorption spectra of the as-synthesized ZnO NPs and PbS QDs reveal that the ZnO NPs have a strong absorption at the wavelength lower than 375 nm, and the PbS QDs absorption peak centered at ~876 nm. The PbS/ZnO reveals a complementary absorption peak from UV to NIR, which is very promising for the broadband photodetector (Fig. 2b). The *I*–*V* curves of the flexible photodetector illuminated with different-wavelength lights (375, 532, 635, 808 and 1,064 nm) are found to be highly sensitive under the broadband light illumination (Fig. 2c), which are related to the PbS QDs, as they act as a strong light absorption layer and NIR sensitizers. The photocurrent increased with the decreasing laser wavelength due to more excitons produced by the high excitation energy. In addition, *I*–*V* characteristics of the devices are quasi-linear because of the ohmic contact between PbS QDs/ZnO NPs channel and Ti/Au electrode (Fig. S6). In comparison, the pure ZnO NPs photodetector shows a photoresponse only in the UV region and a weak response in Vis and NIR region (Fig. S7a), while the pure PbS QDs photodetector exhibits high dark current (Fig. S7b) and low on/off ratios compared with the PbS QDs/ZnO NPs heterostructre based photo-

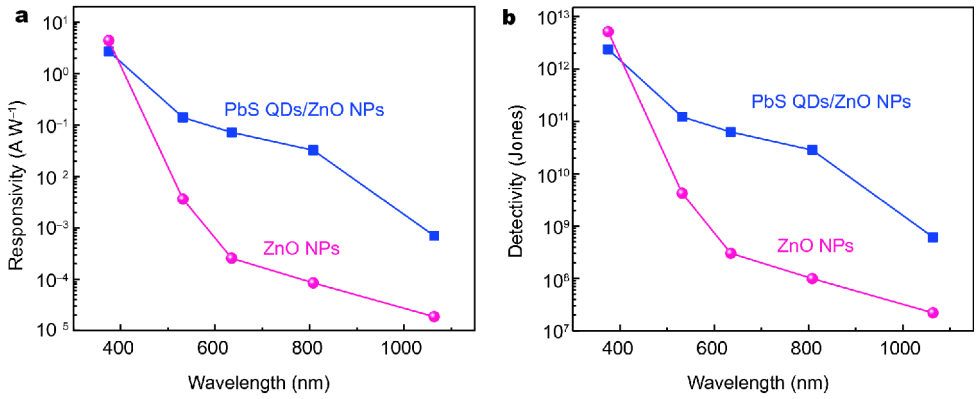

Figure 3 Photoelectric performance comparison for the photodetectors. (a) The responsivity, and (b) detectivity for PbS QDs/ZnO NPs and pure ZnO NPs photodetectors under different wavelength light illumination at 5 V bias.

detector. The *I*–*V* characteristics of pure ZnO NPs films, PbS/ZnO heterostructre, and pure PbS QDs films photodetector under dark and 375 nm light illumination were also investigated (Fig. S8). Both the pure ZnO NPs films and PbS/ZnO heterostructure exhibit an enhanced photocurrent with 375 nm (UV) light illumination. Compared to pure ZnO NPs devices, the optoelectronic performance of heterostructure shows a slight decrease with UV light illumination. The first reason for the slightly decreased photocurrent of the heterostructure is the formation of PbS QDs thin film on the top of the ZnO NPs films, which weakened the UV light absorption for ZnO NPs. The other reason is that the lower carrier mobility of the PbS QDs in the heterostructure films leads to the slight decrease of photocurrent compared with the pure ZnO NPs devices in the UV range. According to previous reports, the higher carrier mobility of ZnO NPs compared with that of PbS QDs will lead to better photoresponse [34,37]. Thus, we deem that the PbS QDs will reduce the carrier mobility of PbS QDs/ZnO NPs heterostructure compared with the pure ZnO NPs devices. This similar phenomenon has been also reported in the similar ZnO NPs based heterostructure photodetectors [26]. Compared to pure PbS QDs film, the PbS/ZnO heterostructure photodetector exhibits an increased photocurrent and decreased dark current. We attribute the increased photocurrent for heterostructure at 375 nm to the photo-generated electron transfer from PbS QDs to ZnO NPs, resulting in electron and hole separation. The I_{light}/I_{dark} ratio and responsivity (R) of the flexible PbS QDs/ZnO NPs photodetector under different wavelength light illumination with the power intensity of ~15.96 mW cm^{-2} at 5 V bias are shown in Fig. 2d. The I_{light}/I_{dark} ratio and responsivity increase with the light wavelength decreasing from 1,064 to 375 nm. The time-resolved photocurrent of the flexible photodetector under 375, 532 and 808 nm light illumination shows that the PbS/ZnO device not only has a broadband photoresponse range (from UV to NIR) and high I_{light}/I_{dark} ratio of 7.08×10^3 (under 375 nm light illumination with light intensity of ~15.96 mW cm^{-2} at 5 V bias), but also displays excellent stability and reproducible switching property (Fig. 2e). The rise and decay time are measured to be about 1.01 s and 1.35 s (Fig. 2f), respectively, which are defined as the time between 10% and 90% of maximum photocurrent.

The comparison of the photoelectric performance between the PbS QDs/ZnO NPs heterostructure and pure ZnO NPs photodetectors was shown in Fig. 3. For the pure ZnO NPs, the photoresponse significantly decreases when the incident light wavelength is longer than 400 nm due to the band gap of ~3.3 eV. However, for the heterostructure, a significantly increased response in the range from Vis to NIR can be observed, which should be attributed to the absorption of PbS QDs. The response for the heterostructures at Vis and NIR range are superior to that of pure ZnO NPs by three orders of magnitude, but the response in the UV range remains, which could be clearly seen in Fig. 3a. It should be noted that the heterostructure devices show a strong photoresponse in Vis-NIR region, consistent with the absorption peak of the PbS QDs/ZnO NPs with a complementary absorption in Vis-NIR region. This clearly indicates that the enhanced photoresponse of the heterostructure in the Vis to NIR range is due to the PbS QDs. The detectivity of PbS QDs/ZnO NPs heterostructure can reach 10^{11} Jones and 10^{10} Jones in the Vis and NIR light range, respectively, but maintain its detectivity of 10^{12} Jones in UV region (Fig. 3b). In addition, the responses of ZnO, PbS and PbS/ZnO based photodetectors under 375 nm light illumination

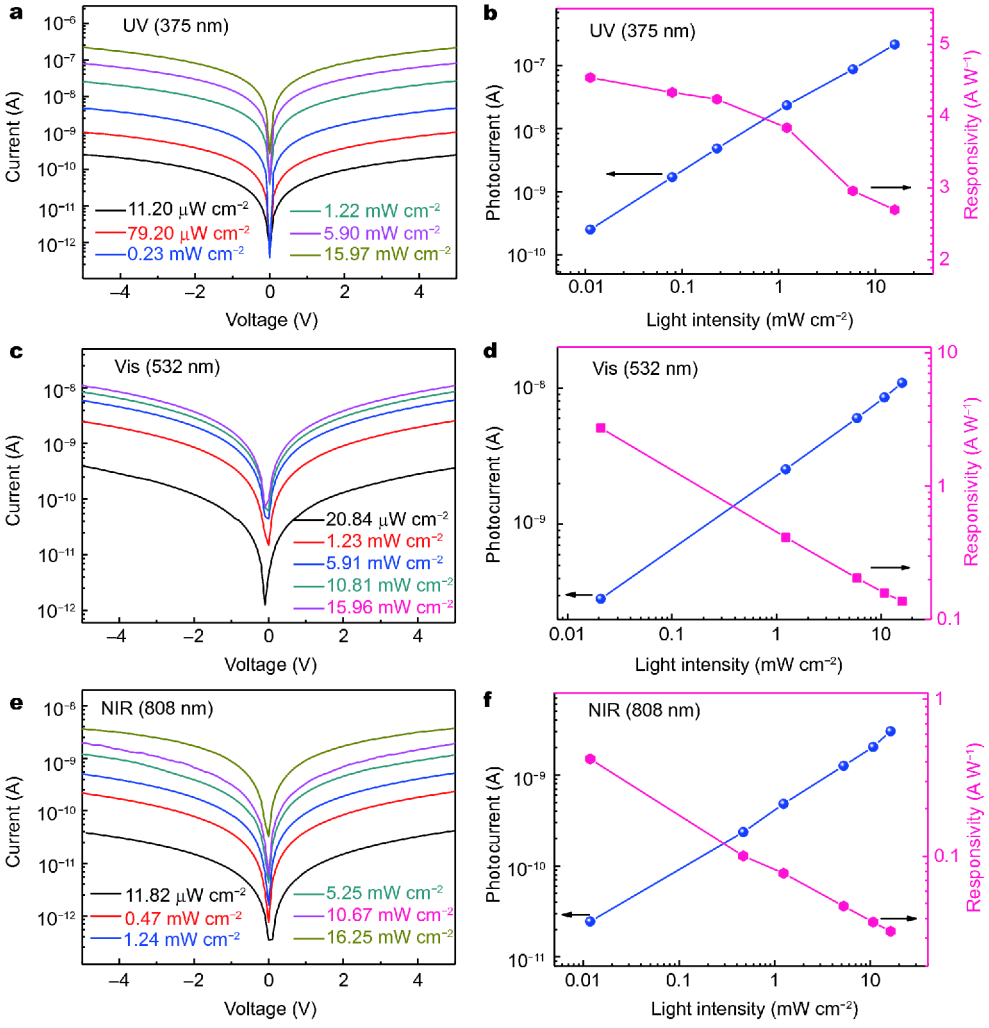

Figure 4 Typical performance of the PbS/ZnO heterostructure based photodetectors. *I*–*V* curves of the photodetector under (a) 375 nm, (c) 532 nm, and (e) 808 nm light with different light intensity illumination, respectively. The photocurrent and responsivity under (b) 375 nm, (d) 532 nm, and (f) 808 nm light as function of light intensity.

were compared in Fig. S9. The response time decreases from 2.27 s (ZnO) and 1.56 s (PbS) to 1.01 s (PbS/ZnO) and the recovery time significantly decreases from original 4.48 s (ZnO) and 2.67 s (PbS) to 1.35 s (PbS/ZnO). Under the light illumination, the electro-hole pairs are photo-induced in the PbS QDs/ZnO NPs heterostructure photodetector. For the heterostructure photodetector, the interface of PbS QDs/ZnO NPs films plays a key role in charge dissociation and transportation. The electrons tend to migrate to the part of ZnO NPs while holes drift to PbS QDs under the built-in electric field. As a result, the recombination rate of the carriers (electrons and holes) further decreases for the heterostructre photodetector, which thus contributes to the photocurrent and response speed. The enhanced photoresponse and response speed are first of all associated with the photo-induced charge transfer between the PbS QDs and ZnO NPs in the heterostructures (More detailed discussion can be found in later).

The typical performances of the PbS/ZnO photodetector are shown in Fig. 4. The *I*–*V* curves of the photodetector show that the photocurrent increases gradually with the increase of the light intensity under different wavelength (375, 532 and 808 nm) light illumination (Fig. 4a, c and e). It also exhibits much stronger and broadband photoresponse than the pure ZnO photodetector (Fig. S7) only in the UV-Vis region and broadens its photoresponse region to the NIR. The photocurrent increases almost linearly with the incident light power intensity under all wavelength light illumi-

nation, while the responsivity decreases (Fig. 4b, d and f). It can be concluded that with low light intensity illumination, photogenerated holes will occupy the surface states and immediately combine with the negative charged oxygen. However, more traps will be further filled by photo-induced charge carriers as the light intensity increases. Since the more traps are fully filled, the extra photoinduced carriers will recombine quickly, thus leading to the saturation of photocurrent [38]. It is consistent with previous reports for photodetectors, indicating that the flexible photodetector is a photon-dependent resistor [39]. The photocurrent can be expressed as following [8]: $I_{ph}=AP^{\theta}$, where I_{ph} is the photocurrent ($I_{ph}=I_{light}-I_{dark}$), A stands for a constant, P is the intensity of incident light, θ is a power law index. According to the power law equation, the θ value can be calculated to be 0.89, 0.58 and 0.76 ($0.5<\theta<1$) under 375, 532 and 808 nm light illuminations, respectively. These results illustrate the loss of the light energy during the conversion from incident light energy to photocurrent, which can be attributed to complex processes in the carrier generation, trapping, and electron-hole recombination in the semiconductor [40,41].

To further evaluate the performance of the photodetector, the responsivity (R) can be described as the following [42,43]: $R=I_{ph}/(PS)$, where P stands for the light intensity, and S is the effective illuminated area. For this flexible photodetector, the effective illuminated area is approximatively 750 μm^2 (the channel width and length of the devices are 150 μm and 5 μm, respectively). The maximum responsivity is calculated to be 4.54 A W^{-1} at 375 nm, 2.73 A W^{-1} at 532 nm, and 0.42 A W^{-1} at 808 nm, respectively. Similarly, the specific detectivity (D^*) is an another important parameter to evaluate the performance of the photodetector, which can be expressed as follow: [30,33] $D^*=R/(2qI_{dark}/S)^{1/2}$, where I_{dark} is the dark current, and q is the absolute value of charge (1.6×10^{-19} C). As shown in Fig. S10, the D^* for the photodetector were measured to be 3.98×10^{12}, 2.39×10^{12} and 3.65×10^{11} Jones at 375 nm, 532 nm, and 808 nm at the bias of 5 V bias, respectively, where D^* is measured in unit of Jones (1 Jones=1 cm Hz$^{1/2}$ W^{-1}). The responsivity of our flexible photodetector reaches a maximum value of ~4.54 A W^{-1} and 3.98×10^{12} Jones at the incident light power intensity of 11.20 μW cm^{-2} under 375 nm light illumination at 5 V bias. The comparison of the performances for some similar photodetectors is listed in Table S1, indicating outstanding optoelectronic performances of our flexible heterostructure based photodetector.

To further evaluate the practical application of the flexible photodetector, the electrical stability under different bending conditions were measured, as shown in Fig. 5. Fig. 5a shows the relationship of photo-current and different bending conditions under 375, 532 and 808 nm light illumination. During the bending process, six different bending conditions of the flexible photodetector with various bending angle from 0° to 150° were studied and labelled as state I–VI, respectively. It can be seen that the photocurrent almost remains nearly unchanged at six different states, indicating that the photocurrents have no significant change with different bending conditions. In order to evaluate the folding endurance property for practical application, the flexible photodetector was bent several times by an automatic linear motor (Fig. S11). Fig. 5b–d show the I–V curves of the PbS QDs/ZnO NPs heterostructure based flexible photodetector without bending and after 100, 200, 300, 400 and 500 times bending under 375, 532 and 808 nm light illumination, respectively. The photocurrent decreases at the beginning of the bending movement while the photocurrent still remains the same order of that after 500 times bending under different wavelength light illumination. The reduced photocurrent at the beginning of the bending process may be attributed to the interspace formation in Ti/Au electrode [8,44]. After bending 500 times, the photocurrent still remains the same order of that before bending under different wavelength light illumination. Fig. 5e–g show the I–t curves of the flexible photodetector without and after bending different times under 375, 532 and 808 nm light illumination, respectively, which exhibits the similar response time even after 500 times bending. These results demonstrate the flexible PbS QDs/ZnO NPs heterostructure photodetector has an excellent mechanical and electrical stability.

Besides the mechanical stability, chemical stability in air and photo-stability are also critical to the practical application of the flexible photodetector. For this reason, we have investigated the chemical stability of the PbS QDs/ZnO QD photodetector in atmospheric environment under different wavelengths (375, 532 and 808 nm) light illumination with light intensity of ~15.96 mW cm^{-2} at 5 V bias. The unencapsulated devices were stored and measured in ambient air at room temperature without any relative humidity control. As shown in Fig. S12a, the spectra responsivity of the device was recorded for 15 days. In the first few days of storage, the device performance was actually improved slightly and subsequently remained stable during the entire testing period. The initial improvement in device performance has been reported for other similar PbS QDs/ZnO NPs devices

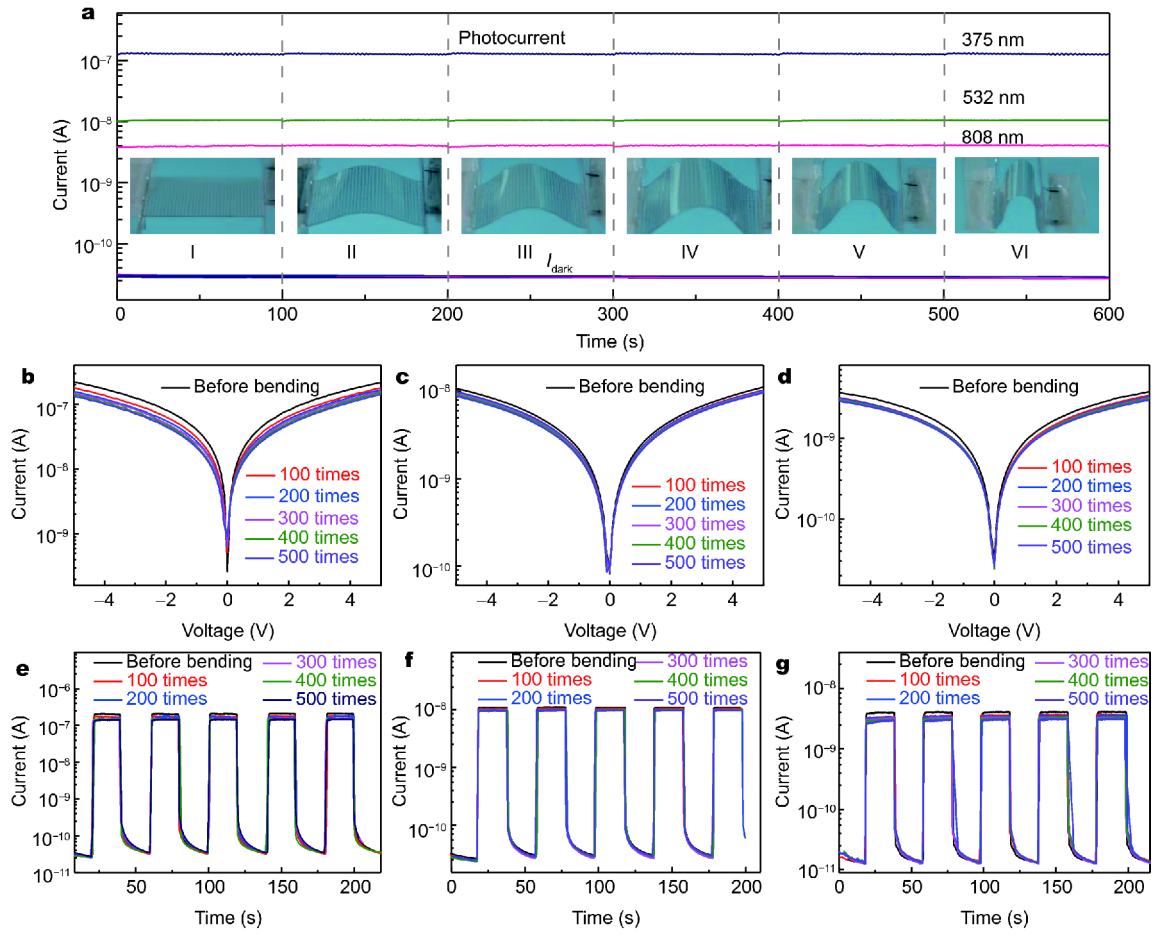

Figure 5 The bending performance of the PbS QDs/ZnO NPs heterostructure based flexible photodetector. (a) Relationship between photocurrent and different bending degree. *I–V* curves of flexible photodetector under (b) 375 nm, (c) 532 nm and (d) 808 nm light illumination without bending and after 100, 200, 300, 400 and 500 times bending. The *I–t* curves of the flexible photodetector under (e) 375 nm, (f) 532 nm and (g) 808 nm light illumination without and after different times bending.

[19,45]. Since ZnO NPs have a large surface area, atmospheric or residual oxygen and moisture can easily bind to their surfaces. For the heterostructure devices, PbS QDs have been spin-coated to passivate the ZnO NPs film from further reactions with oxygen and moisture. Thus, photoexcitation and surface passivation can improve the performance of the devices [46]. In order to investigate the illumination stability, the performance of the heterostructure has been recorded under 100 mW cm^{-2} simulated AM 1.5G illumination with different illumination times in nitrogen atmosphere, as shown in Fig. S12b. It is found that PbS QDs/ZnO NPs photodetector shows excellent photo-stability, even after 72 h of continuous illumination.

To understand the working mechanism and the performance enhancement of the flexible PbS/ZnO heterostructure based photodetector, we further performed PL measurements on PbS and PbS/ZnO heterostructure (Fig. 6a), respectively. As we know, PL intensity is mainly determined by dipole-dipole couplings or charge transfer. The dipole-dipole interaction arising from the dipole moments between acceptor and donor usually takes place among molecules [47–48]. When it comes to charge transfer, the nonradioactive rate of two adjacent photosensitive materials can be simultaneously increased, arising from light emission quenching from all transitions [16]. Compared with the PbS-only PL spectrum (emission center located at ~995 nm, corresponding to PbS near band-edge emission), a significant decrease in the band-to-band transition peak obviously occurs in the PbS/ZnO heterostructure. This phenomenon further indicates that a great proportion of the photo-generated carriers may transfer between PbS and ZnO. Moreover, it also illustrates that the PbS QDs/ZnO NPs heterostructure may

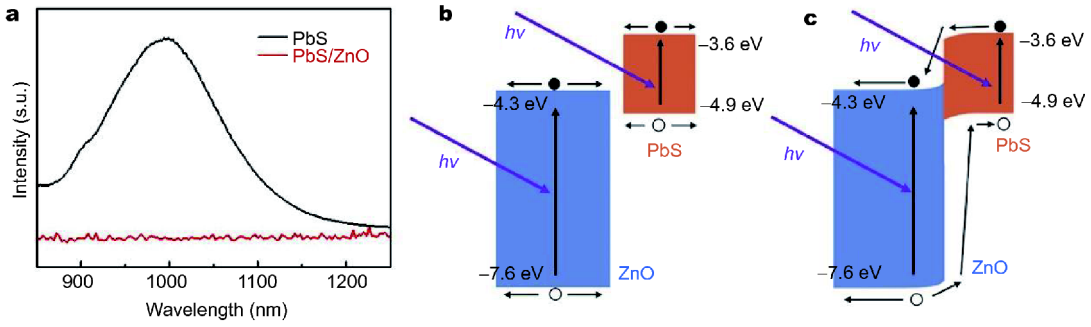

Figure 6 Enhancement mechanism of the PbS QDs/ZnO NPs heterostructure based photodetector. (a) Photoluminescence measured for PbS and PbS/ZnO heterostructure. Energy bandgap diagrams of the PbS/ZnO heterostructure under light illumination (b) before and (c) after contact.

prevent or reduce the photo-generated carrier recombination [16,49]. The recombination rate of the electron-hole pairs will decrease due to the spatial separation of the photo-induced carriers, which leads to a significant increase of the carrier density in heterostructure. The PL spectra of the pure ZnO NPs, PbS QDs/ZnO NPs and pure PbS QDs from 340 to 850 nm are obtained with excitation of 325 nm He-Cd laser, as shown in Fig. S13. Besides the band-edge emission at ~360 nm, an emission around 550 nm is also observed in pure ZnO NPs. It mainly originates from the surface oxygen vacancies known as deep donors [50]. PbS/ZnO heterostructure has a noteworthy decrease in the intensity of the emission peaks compared to the bare ZnO NPs film. It further demonstrates that the large proportion of the photo-generated carriers may transfer between PbS and ZnO. Energy bandgap diagrams of the PbS/ZnO heterostructure under light illumination are shown in Fig. 6b, c. Before contact, under illumination with an incident light energy larger than the band gap (E_g) of the semiconductor, electron-hole pairs are photo-induced, while holes are readily trapped by the surface with the unpaired electrons. In PbS/ZnO heterostructure, unpaired electrons tend to transfer from PbS layer to ZnO layer and the holes will transfer from ZnO to PbS due to band alignment under light illumination. Thus, the formation of heterostructure facilitates charge carrier transport and enhances the performance of the photodetector.

CONCLUSIONS

In conclusion, we have synthesized the PbS QDs/ZnO NPs heterostructure based flexible photodetector *via* a facile and low-cost solution-processed approach. The flexible heterostructure photodetector exhibits a broadband photoresponse range from UV-Vis to NIR with high current on/off ratio of 7.08×10^3, 3.68×10^2 and 1.23×10^2 under 375, 532, and 808 nm light illumination, respectively. Compared with pure ZnO NPs, the heterostructure shows an improvement of responsivity in Vis and NIR range by three orders of magnitude, and maintains its response performance in the UV range simultaneously. It shows a spectra responsivity and detectivity of 4.54 A W^{-1} and 3.98×10^{12} Jones at 375 nm, 2.73 A W^{-1} and 2.39×10^{12} Jones at 532 nm, and 0.42 A W^{-1} and 3.65×10^{11} Jones at 808 nm respectively. In addition, the flexible photodetector displays excellent durability and stability even after 500 times bending cycles. We envisage that this work paves a promising way for constructing next-generation high-performance flexible and broadband optoelectronic devices.

Received 24 April 2018; accepted 8 June 2018; published online 28 June 2018

1 Wang X, Shi G. Flexible graphene devices related to energy conversion and storage. Energy Environ Sci, 2015, 8: 790–823
2 Gong X, Tong M, Xia Y, *et al.* High-detectivity polymer photodetectors with spectral response from 300 nm to 1450 nm. Science, 2009, 325: 1665–1667
3 Arnold MS, Zimmerman JD, Renshaw CK, *et al.* Broad spectral response using carbon nanotube/organic semiconductor/C_{60} photodetectors. Nano Lett, 2009, 9: 3354–3358
4 Yoo J, Jeong S, Kim S, *et al.* A stretchable nanowire UV-Vis-NIR photodetector with high performance. Adv Mater, 2015, 27: 1712–1717
5 Hu X, Zhang X, Liang L, *et al.* High-performance flexible broadband photodetector based on organolead halide perovskite. Adv Funct Mater, 2014, 24: 7373–7380
6 Kang Y, Liu HD, Morse M, *et al.* Monolithic germanium/silicon avalanche photodiodes with 340 GHz gain–bandwidth product. Nat Photonics, 2009, 3: 59–63
7 Lou Z, Shen G. Flexible photodetectors based on 1D inorganic nanostructures. Adv Sci, 2016, 3: 1500287
8 Peng M, Wen Z, Shao M, *et al.* One-dimensional CdS_xSe_{1-x} nanoribbons for high-performance rigid and flexible photodetectors. J Mater Chem C, 2017, 5: 7521–7526
9 Tamalampudi SR, Lu YY, Kumar U. R, *et al.* High performance

and bendable few-layered InSe photodetectors with broad spectral response. Nano Lett, 2014, 14: 2800–2806
10 Chen S, Teng C, Zhang M, *et al.* A flexible UV-Vis-NIR photodetector based on a perovskite/conjugated-polymer composite. Adv Mater, 2016, 28: 5969–5974
11 Ghezzi D, Antognazza MR, Maccarone R, *et al.* A polymer optoelectronic interface restores light sensitivity in blind rat retinas. Nat Photonics, 2013, 7: 400–406
12 Gutruf P, Walia S, Sriram S, *et al.* Visible-blind UV imaging with oxygen-deficient zinc oxide flexible devices. Adv Electron Mater, 2015, 1: 1500264
13 Gomathi PT, Sahatiya P, Badhulika S. Large-area, flexible broadband photodetector based on ZnS-MoS_2 hybrid on paper substrate. Adv Funct Mater, 2017, 27: 1701611
14 Wang X, Song W, Liu B, *et al.* High-performance organic-inorganic hybrid photodetectors based on P3HT:CdSe nanowire heterojunctions on rigid and flexible substrates. Adv Funct Mater, 2013, 23: 1202–1209
15 Liu YL, Yu CC, Lin KT, *et al.* Transparent, broadband, flexible, and bifacial-operable photodetectors containing a large-area graphene–gold oxide heterojunction. ACS Nano, 2015, 9: 5093–5103
16 Gao T, Zhang Q, Chen J, *et al.* Performance-enhancing broadband and flexible photodetectors based on perovskite/ZnO-nanowire hybrid structures. Adv Opt Mater, 2017, 5: 1700206
17 Tang J, Sargent EH. Infrared colloidal quantum dots for photovoltaics: fundamentals and recent progress. Adv Mater, 2011, 23: 12–29
18 Wadia C, Alivisatos AP, Kammen DM. Materials availability expands the opportunity for large-scale photovoltaics deployment. Environ Sci Technol, 2009, 43: 2072–2077
19 Manders JR, Lai TH, An Y, *et al.* Low-noise multispectral photodetectors made from all solution-processed inorganic semiconductors. Adv Funct Mater, 2014, 5: 7205–7210
20 Jean J, Chang S, Brown PR, *et al.* ZnO nanowire arrays for enhanced photocurrent in PbS quantum dot solar cells. Adv Mater, 2013, 25: 2790–2796
21 Lee JW, Kim DY, Baek S, *et al.* Inorganic UV-Visible-SWIR broadband photodetector based on monodisperse PbS nanocrystals. Small, 2016, 12: 1328–1333
22 Luther JM, Gao J, Lloyd MT, *et al.* Stability assessment on a 3% bilayer PbS/ZnO quantum dot heterojunction solar cell. Adv Mater, 2010, 22: 3704–3707
23 Pal BN, Robel I, Mohite A, *et al.* High-sensitivity p-n junction photodiodes based on PbS nanocrystal quantum dots. Adv Funct Mater, 2012, 22: 1741–1748
24 Lee JW, Kim DY, So F. Unraveling the gain mechanism in high performance solution-processed PbS infrared PIN photodiodes. Adv Funct Mater, 2015, 25: 1233–1238
25 Sun L. Employing ZnS as a capping material for PbS quantum dots and bulk heterojunction solar cells. Sci China Mater, 2016, 59: 817–824
26 Jin Z, Zhou Q, Chen Y, *et al.* Graphdiyne: ZnO nanocomposites for high-performance UV photodetectors. Adv Mater, 2016, 28: 3697–3702
27 Xue M, Zhou H, Xu Y, *et al.* High-performance ultraviolet-visible tunable perovskite photodetector based on solar cell structure. Sci China Mater, 2017, 60: 407–414
28 Bai S, Wu W, Qin Y, *et al.* High-performance integrated ZnO nanowire UV sensors on rigid and flexible substrates. Adv Funct Mater, 2011, 21: 4464–4469
29 De Iacovo A, Venettacci C, Colace L, *et al.* PbS colloidal quantum dot photodetectors operating in the near infrared. Sci Rep, 2016, 6: 37913
30 Ren Z, Sun J, Li H, *et al.* Bilayer PbS quantum dots for high-performance photodetectors. Adv Mater, 2017, 29: 1702055
31 Gong M, Liu Q, Cook B, *et al.* All-printable ZnO quantum dots/graphene van der Waals heterostructures for ultrasensitive detection of ultraviolet light. ACS Nano, 2017, 11: 4114–4123
32 Osedach TP, Zhao N, Geyer SM, *et al.* Interfacial recombination for fast operation of a planar organic/QD infrared photodetector. Adv Mater, 2010, 22: 5250–5254
33 Zheng Z, Gan L, Zhang J, *et al.* An enhanced UV-Vis-NIR and flexible photodetector based on electrospun ZnO nanowire array/PbS quantum dots film heterostructure. Adv Sci, 2017, 4: 1600316
34 Hu C, Dong D, Yang X, *et al.* Synergistic effect of hybrid PbS quantum dots/2D-WSe_2 toward high performance and broadband phototransistors. Adv Funct Mater, 2017, 27: 1603605
35 Hines MA, Scholes GD. Colloidal PbS nanocrystals with size-tunable near-infrared emission: observation of post-synthesis self-narrowing of the particle size distribution. Adv Mater, 2003, 15: 1844–1849
36 Zhang Y, Xu Y, Ford MJ, *et al.* Thermally stable all-polymer solar cells with high tolerance on blend ratios. Adv Energy Mater, 2018, 270: 1800029
37 Sun B, Sirringhaus H. Solution-processed zinc oxide field-effect transistors based on self-assembly of colloidal nanorods. Nano Lett, 2005, 5: 2408–2413
38 Zhou X, Zhang Q, Gan L, *et al.* High-performance solar-blind deep ultraviolet photodetector based on individual single-crystalline Zn_2GeO_4 nanowire. Adv Funct Mater, 2016, 26: 704–712
39 Li QL, Li Y, Gao J, *et al.* High performance single In_2Se_3 nanowire photodetector. Appl Phys Lett, 2011, 99: 243105
40 Kind H, Yan H, Messer B, *et al.* Nanowire ultraviolet photodetectors and optical switches. Adv Mater, 2002, 14: 158–160
41 Liu F, Shimotani H, Shang H, *et al.* High-sensitivity photodetectors based on multilayer GaTe flakes. ACS Nano, 2014, 8: 752–760
42 Lei S, Ge L, Najmaei S, *et al.* Evolution of the electronic band structure and efficient photo-detection in atomic layers of InSe. ACS Nano, 2014, 8: 1263–1272
43 Feng W, Zheng W, Chen XS, *et al.* Solid-state reaction synthesis of a InSe/$CuInSe_2$ lateral p–n heterojunction and application in high performance optoelectronic devices. Chem Mater, 2015, 27: 983–989
44 Xie X, Shen G. Single-crystalline In_2S_3 nanowire-based flexible visible-light photodetectors with an ultra-high photoresponse. Nanoscale, 2015, 7: 5046–5052
45 Wang Y, Lu K, Han L, *et al. In situ* passivation for efficient PbS quantum dot solar cells by precursor engineering. Adv Mater, 2018, 30: 1704871
46 Chen S, Small CE, Amb CM, *et al.* Inverted polymer solar cells with reduced interface recombination. Adv Energy Mater, 2012, 2: 1333–1337
47 Prins F, Goodman AJ, Tisdale WA. Reduced dielectric screening and enhanced energy transfer in single- and few-layer MoS_2. Nano Lett, 2014, 14: 6087–6091
48 Barnes WL, Andrew P. Quantum optics: Energy transfer under control. Nature, 1999, 400: 505–506
49 Tian W, Zhai T, Zhang C, *et al.* Low-cost fully transparent ultraviolet photodetectors based on electrospun ZnO-SnO_2 heterojunction nanofibers. Adv Mater, 2013, 25: 4625–4630

50 Dao TD, Dang CTT, Han G, *et al.* Chemically synthesized nanowire TiO_2/ZnO core-shell p-n junction array for high sensitivity ultraviolet photodetector. Appl Phys Lett, 2013, 103: 193119

Acknowledgements The work was funded by the National Natural Science Foundation of China (U1432249), the National Key R&D Program of China (2017YFA0205002), the Priority Academic Program Development of Jiangsu Higher Education Institutions (PAPD). This is also a project supported by Collaborative Innovation Center of Suzhou Nano Science & Technology and Joint International Research Laboratory of Carbon-Based Functional Materials and Devices. Wen Z thanks the support from China Postdoctoral Science Foundation (2017M610346) and Natural Science Foundation of Jiangsu Province of China (BK20170343).

Author contributions Peng M, Wang Y and Shen Q have contributed equally to this work. Peng M designed and fabricated the devices. Wang Y synthesized the nanomaterials. Shen Q, Xie X and Zheng H performed the structure and morphology characterization. Peng M wrote the paper with support from Ma W, Wen Z and Sun X. All authors contributed to the experiment data discussion.

Conflict of interest The authors declare no conflict of interest.

Supplementary information Supporting data are available in the online version of the paper.

Mingfa Peng received his BSc degree in materials chemistry from Hubei Engineering University in 2008 and MSc degree in materials science from Soochow University in 2011, respectively. He is currently a PhD candidate in the Institute of Functional Nano & Soft Materials (FUNSOM), Soochow University. His research focuses primarily on nanomaterial-based device fabrication and self-powered active photodetector.

Zhen Wen received his BSc degree in materials science and engineering from China University of Mining and Technology (CUMT) in 2011 and PhD degree in materials physics and chemistry from Zhejiang University (ZJU) in 2016. During 2014–2016, he was supported by the program of China Scholarship Council (CSC) as a joint PhD student in Georgia Institute of Technology (GT). He joined in the Institute of Functional Nano & Soft Materials (FUNSOM), Soochow University as an assistant professor since the end of 2016. His main research interest focuses on triboelectric nanogenerator based energy harvesting and self-powered sensing system.

Xuhui Sun is a full professor at the Institute of Functional Nano & Soft Materials (FUNSOM) at Soochow University. He received his PhD degree from the City University of Hong Kong in 2002. He performed postdoctoral research at the University of Western Ontario, Canada from 2003 to 2005 and at NASA Ames Research Center, USA from 2005 to 2007. He became a research scientist at NASA and adjunct assistant professor at Santa Clara University in 2007. His research interest includes nanoelectronics, energy harvesting, nanosensors, and the development and application of synchrotron radiation techniques.

基于硫化铅量子点和氧化锌纳米颗粒异质结的高性能柔性和宽波段光电探测器

彭明发, 汪永杰, 沈青青, 谢欣凯, 郑和闯, 马万里, 文震*, 孙旭辉*

摘要 柔性和宽波段的光电探测器在可折叠显示、光通信和环境监测等方面有潜在的应用, 因而引起广泛的关注. 本文基于硫化铅量子点和氧化锌纳米颗粒异质结制备了柔性光电探测器. 该器件表现出从紫外光到近红外光的宽波段光电响应性能. 在375 nm紫外光照射下, 该器件的电流开关比高达7.08×10^3. 与单纯的氧化锌纳米颗粒器件相比, 基于异质结的光电探测器的响应度在可见光和近红外光区间增加了三个数量级, 同时维持了器件在紫外光范围内的性能不变. 同时, 基于异质结的器件的响应度和探测率高达4.54 A W^{-1}和3.98×10^{12} Jones. 此外, 所研制的柔性光电探测器在经过数百次的折叠后, 仍表现出了良好的机械和电学稳定性. 本工作为下一代柔性和宽波段光电子器件的研究做了一个初步探索.

